Available online at www.sciencedirect.com
SCIENCE DIRECT®
Coastal Engineering 51 (2004) 1–15
Coastal Engineering
An International Journal for Coastal, Harbour and Offshore Engineers
www.elsevier.com/locate/coastaleng

The applicability of the shallow water equations for modelling violent wave overtopping

J.B. Shiach[a,*], C.G. Mingham[a], D.M. Ingram[a], T. Bruce[b]

[a] Centre for Mathematical Modelling and Flow Analysis, Manchester Metropolitan University, Chester Street, Manchester M1 5GD, UK
[b] School of Engineering and Electronics, The University of Edinburgh, Kings Buildings, Mayfield Road, Edinburgh EH9 3JL, UK

Received 26 March 2003; received in revised form 1 October 2003; accepted 4 November 2003

Abstract

The shallow water equations (SWE) have been used to model a series of experiments examining violent wave overtopping of a near-vertical sloping structure with impacting wave conditions. A finite volume scheme was used to solve the shallow water equations. A monotonic reconstruction method was applied to eliminate spurious oscillations and ensure proper treatment of bed slope terms. Both the numerical results and physical observations of the water surface closely followed the relevant Rayleigh probability distributions. However, the numerical model overestimated the wave heights and suffered from the lack of dispersion within the shallow water equations. Comparisons made on dimensionless parameters for the overtopping discharge and percentage of waves overtopping between the numerical model and the experimental observations indicated that for the lesser impacting waves, the shallow water equations perform satisfactorily and provide a good alternative to computationally more expensive methods.

Keywords: Violent wave overtopping; Shallow water equations; Finite volume method; Surface gradient method

1. Introduction

Violent wave overtopping occurs when waves break against sea walls, throwing water up and over the top. Of the hundreds of kilometres of coastal defences in Britain, a significant proportion have roads, railways and footpaths running alongside. Violent overtopping events have been known to wash people, cars and trains into the sea and represent a threat to human life and property.

Wave overtopping has been studied extensively over the past 30 years. Goda et al. (1975), Owen (1982) and Franco et al. (1994) all present data and guidance on overtopping volumes for a variety of sloping and vertical structures. Owen and Franco et al. focus primarily upon cases where waves do not break (pulsating or nonimpulsive conditions). While Goda's data includes violent or impulsive conditions, these are not treated separately. Besley et al. (1998) and Pearson et al. (2001) have used observations from either physical models or field data to gain a greater understanding of violent, impulsive overtopping.

* Corresponding author. Tel.: +44-161-247-1515; fax: +44-161-247-1483.
E-mail address: j.shiach@mmu.ac.uk (J.B. Shiach).

0378-3839/$ - see front matter © 2004 Elsevier B.V. All rights reserved.
doi:10.1016/j.coastaleng.2003.11.001

Guidance on mean and wave-on-wave overtopping volumes under violent conditions is now established, but for simple structures and standard sea spectra only.

Violent overtopping events are difficult to model using current numerical methods. Ideally, the use of the well-known Navier–Stokes equations would provide a good model of the overtopping events. However, numerical solvers for these equations require extensive computational resources, and until computers are developed that can allow for a model based on the Navier–Stokes equations to be practical, an alternative method is required.

A depth-averaged formulation of the Navier–Stokes equations exists in the shallow water equations (SWE). As the SWE are depth averaged, any vertical velocity is neglected. Thus, these equations, in theory, may not be suitable as a basis for a numerical model for violent wave overtopping where vertical velocities are a major feature. However, SWE models are easy to implement and computationally efficient. Therefore, before discarding them altogether, an analysis of the limitations of the SWE model is required.

Existing models that make use of the SWE to model wave runup and overtopping include ODIFLOCS (van Gent, 1994, 1995) and ANEMONE (Dodd, 1998). These models have been used to give predictions of wave runup and overtopping of sea dikes where wave conditions are less impacting and violent overtopping is less likely to occur.

This paper examines the validity of a numerical model based on the SWE to model violent wave overtopping of sea walls.

2. Numerical model

The shallow water equations (SWE) in one dimension can be expressed as

$$\frac{\partial}{\partial t}\boldsymbol{U}+\frac{\partial}{\partial x}\boldsymbol{F}(\boldsymbol{U})=\boldsymbol{S} \tag{1}$$

where

$$\boldsymbol{U}=\begin{pmatrix}\phi\\ \phi u\end{pmatrix},\quad \boldsymbol{F}(\boldsymbol{U})=\begin{pmatrix}\phi u\\ \phi u^2+\frac{1}{2}\phi^2\end{pmatrix},$$
$$\boldsymbol{S}=\begin{pmatrix}0\\ g\phi\ \ \partial H/\partial x\end{pmatrix}, \tag{2}$$

and $\phi=gh$ is the geopotential; h is the water depth; $g=9.81\ \mathrm{m\ s^{-2}}$ is the acceleration due to gravity; u is the depth average velocity in the x-direction, and H is the distance between a fixed reference level and the bed surface elevation (see Fig. 1). In this form, $\boldsymbol{U}$ represents the vector of conserved variables, $\boldsymbol{F}(\boldsymbol{U})$ the flux vector function, and $\boldsymbol{S}$ is the vector of source terms.

The SWE are a hyperbolic system of partial differential equations that can admit discontinuities into the solution. These can be difficult to model as spurious oscillations created by the numerical scheme around the area of the discontinuity tend to contaminate the solution and eventually render any results worthless. Therefore, for a scheme to be considered applicable when solving the SWE, it must be able to satisfactorily deal with discontinuous behaviour. The

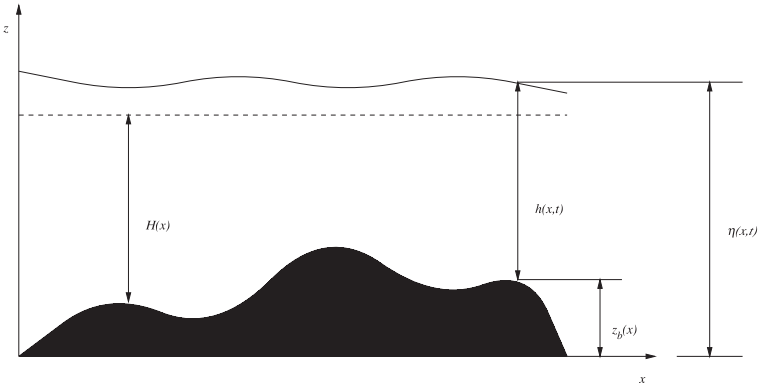

Fig. 1. Definition sketch for bed topography.

MUSCL–Hancock finite volume scheme (van Leer, 1985) has been chosen by the authors as it has been extensively tested over a range of demanding test cases (Mingham and Causon, 1998; Hu et al. 2000) and performed admirably in all. The scheme is a high-resolution Godunov-type scheme incorporating the HLL Riemann solver (Harten et al. 1983) to provide solutions to the local Riemann problems at the cell interfaces.

2.1. The MUSCL–Hancock scheme

The MUSCL–Hancock scheme is a two-stage predictor–corrector method. The predictor stage is given as

$$\boldsymbol{U}_{ij}^{n+1/2} = \boldsymbol{U}_{ij}^{n} - \frac{\Delta t}{2A}\left(\sum_{m=1}^{M} \boldsymbol{F}(\boldsymbol{U}_m)\cdot \boldsymbol{L}_m - A\boldsymbol{S}_{ij}^{n}\right), \tag{3}$$

where n is the time step counter; ij is the cell index; Δt is the step; A is the cell area; $\boldsymbol{L}_m$ is the cell side vector defined as the cell side multiplied by the outward pointing unit normal vector; M is the number of sides of the cell ij. The fluxes at the cell interfaces m ($\boldsymbol{F}(\boldsymbol{U}_m)$) are calculated using slope limited gradients based upon neighbouring cell data (Section 2.1.1).

The corrector stage provides a fully conservative solution over one time step and is given as

$$\boldsymbol{U}_{ij}^{n+1} = \boldsymbol{U}_{ij}^{n} - \frac{\Delta t}{A}\left(\sum_{m=1}^{M} \boldsymbol{F}(\boldsymbol{U}_m^L, \boldsymbol{U}_m^R)^{n+1/2}\cdot \boldsymbol{L}_m - A\boldsymbol{S}_{ij}^{n+1/2}\right), \tag{4}$$

where the flux vector $\boldsymbol{F}(\boldsymbol{U}_m^L,\boldsymbol{U}_m^R)$ are the solutions to the local Riemann problems at each time step calculated using the HLL approximate Riemann solver (see Section 2.1.2). $\boldsymbol{U}_m^L$ and $\boldsymbol{U}_m^R$ are the conserved variables at the left and right side of each cell interface, respectively.

A full description and extensive validation of the MUSCL–Hancock scheme can be found in Mingham and Causon (1998).

2.1.1. MUSCL reconstruction

MUSCL (Monotonic Upwind Schemes for Conservation Laws) schemes use the values of the conserved variables at the cells immediately adjacent to the cell i to calculate a slope-limited gradient which ensures that there is no over/undershoots at the cell interfaces, $(i \pm 1/2)$ (Toro, 1997). Here, the authors have used the well-known van Leer slope limiter function which is given in Hirsch (1998).

The values of the conserved variables ϕ and ϕu can be found at the cell interfaces by using linear interpolation. For example, the values of the geopotential at the left- and right-hand side of the cell interface $(i-1/2)$ are

$$\phi_{i-1/2}^{L} = \phi_{i-1} + \frac{1}{2}\Delta x_{i-1}\delta\phi_{i-1},$$
$$\phi_{i-1/2}^{R} = \phi_{i} - \frac{1}{2}\Delta x_{i}\delta\phi_{i}, \tag{5}$$

where $\delta\phi_i$ are the slope limited gradients of ϕ_i and

$$\Delta x_i = x_{i+1/2} - x_{i-1/2}. \tag{6}$$

2.1.2. HLL approximate Riemann solver

The corrector stage of the Hancock scheme requires the solution to a local Riemann problem at every cell interface. The Riemann solver used here was developed by Harten et al. (1983) (HLL) and has shown to be accurate and robust in practice (Mingham and Causon, 1998) and considerably less computationally expensive than an exact Riemann solver. The wave speed calculations used here can be found in Davis (1988) for a wet bed and Fraccarollo and Toro (1995) for a dry bed.

2.1.3. Time step calculation

To ensure that the time marching scheme remains stable, a maximum allowable time step calculation based upon the stability condition developed by Courant, Friedrichs and Lewy (CFL) is applied (Morton and Mayers, 1994). The time step Δt is given by

$$\Delta t = v \min_i\left(\frac{\Delta x_i}{|u_i| + \sqrt{\phi_i}}\right), \tag{7}$$

where v is the Courant number $(0 < v \le 1)$. For all numerical solutions presented here, a Courant number

of $v=0.65$ was used throughout to ensure scheme stability.

2.2. The surface gradient method

The numerical scheme presented in Section 2.1 solves the homogeneous form of the SWE where applications are mainly limited to flat-bed shock and bore wave propagation problems. However, the inclusion of the source terms that model bed topography ensure more realistic formulations applicable to problems such as wave runup and overtopping on a sloping beach and tidal flows in coastal water regions. It has been found that for a conservative scheme a naïve numerical treatment of source terms may lead to nonphysical behaviour of the fluid (Leveque, 1998).

The numerical treatment of source terms has received particular attention in the last few years with a variety of different methods proposed. Garcia-Navarro and Vázquez-Cendón (2000) proposed an upwind scheme which uses an extension of the formulation of Roe's scheme. Another approach was proposed by Hu et al. (2000), in which the authors used the MUSCL–Hancock scheme to solve the inviscid SWE along with an ODE solver (Euler) for the treatment of the source terms. Both of the methods described above performed well on standard test cases. However, they did suffer from being overly complicated. Zhou et al. (2001) developed a Surface Gradient Method (SGM) to deal with the treatment of the source terms that requires very few alterations to the MUSCL–Hancock scheme. The SGM was shown to give excellent agreement with known solutions to standard test cases chosen to examine the scheme's ability to model both transcritical flow and steady-state problems.

Traditional MUSCL schemes use the conserved variables ϕ and ϕu to approximate the fluxes at the cell interfaces such as

$$\phi_{i\pm1/2} = \phi_i \pm \frac{1}{2}\Delta x_i \delta\phi_i,$$
$$(\phi u)_{i\pm1/2} = (\phi u)_i \pm \frac{1}{2}\Delta x_i \delta(\phi u)_i, \tag{8}$$

where $i\pm1/2$ are the cell interfaces; Δx is the cell width and $\delta\phi_i$ and $\delta(\phi u)_i$ are the slope-limited gradients across cell i. The SGM approach uses the water surface elevation as the basis for the MUSCL reconstruction instead of the geopotential. The water surface elevation, η_i, is defined by

$$\eta_i = h_i + z_{bi}, \tag{9}$$

where h_i and z_{bi} are the water height and bed surface elevation, respectively (Fig. 1). The reconstruction process is then applied by using

$$\phi_{i\pm1/2} = g\left(\eta_i \pm \frac{1}{2}\Delta x_i \delta\eta_i - z_{bi\pm1/2}\right) \tag{10}$$

This approach ensures that any errors that are caused by the difference between the gradient of the water height, $h(x,t)$, and the gradient of the bed slope, $z_b(x)$, do not affect the solution. The SGM is fully conservative so long as a centred discretisation of the source terms is used. When using the SGM, the bed surface elevation, z_{bi} is calculated by averaging the bed elevation at the cell interfaces.

A full description of the SGM together with a formal proof of the conservative properties and validation can be found in Zhou et al. (2001).

3. Violent wave overtopping

The more violent impact of water waves on sea walls cause velocities and pressures much larger then those associated with the wave's propagation under gravity (Peregrine, 2002), and it is under these conditions that violent wave overtopping can occur. A study into violent wave overtopping was the focus of the VOWS (Violent Overtopping by Waves at Sea walls) project funded by the EPSRC (Engineering and Physical Sciences Research Council). As part of the VOWS project, physical model tests of violent wave overtopping were carried out in a wave channel at the University of Edinburgh.

Allsop et al. (1995) developed a parameter (h^*) that measures the type of wave interaction (and therefore, the type of overtopping) with vertical walls. The h^* parameter is given as

$$h^* = \frac{h}{H_s}\left(\frac{2\pi h}{gT_m^2}\right), \tag{11}$$

where h is the wave height at the toe of the structure; $H_s = H_{1/3}$ (the mean of the top one-third

wave heights) is the significant wave height, $g = 9.81$ m s^{-2} is the acceleration due to gravity and T_m is the mean wave period. When $h^* > 0.3$, the waves reflect from the vertical structure, and any overtopping is likely to be gentle 'green water' overtopping. When $h^* \leq 0.3$, impacting waves begin to prevail and ultimately dominate, resulting in violent wave overtopping.

3.1. The Edinburgh wave flume experiments

The wave flume that was used to carry out the physical modelling is approximately 20 m in length by 0.4 m wide with an absorbing flap-type wave generator located at one end (Fig. 2). The operating water depth is 0.7 m (intermediate depth at the wave generator). The basic bathymetry of the wave flume consists of a 1:10 sloping beach on which is placed a 10:1 battered wall. The battered wall is placed so that the water depth at the toe of the structure, h, is 0.09 m. Eight wave gauges that record water surface elevation are placed at 1.0, 2.0, 3.0, 4.25, 5.5, 6.75, 8.0 and 11.21 m away from the battered wall and record water depth at a rate of 100 Hz (Fig. 3). The wave generator produced 1024-second sequences of waves from the JONSWAP spectrum with $\gamma = 3.3$, representing sequences consisting of $\sim$ 1000 waves. In all, 15 runs of the experiment were carried out using this configuration that produced h^* values ranging from 0.03 to 0.1.

Table 1 contains the significant wave height (H_s) measured at the toe of the battered wall, the mean wave period (T_m), the h^* parameter and the dimensionless freeboard R_h (see Section 3.4) for the 15 runs of the experiment.

3.2. Numerical model of the Edinburgh wave flume experiments

For the numerical modelling of the Edinburgh wave flume experiments, a reduced solution domain starting at 2.0 m away from the battered wall was used to minimise the energy loss that may occur as the waves propagate up the flume. The total length of the numerical flume was 2.1 m which was discretised into 100 computational cells ($\Delta x = 0.021$ m). The water surface elevation recorded at the gauge placed 2.0 m away from the battered wall serves as the boundary condition for the water depth at the left-hand boundary, whilst the velocity was assumed to be the same as that of the first computational cell in from the left-hand boundary. This boundary condition takes into account both incident waves and reflecting waves from the structure. A study carried out by Richardson et al. (2001) showed that this boundary condition provides values of the water surface and velocity that are 99% and 85% accurate, respectively, when compared to a moving boundary model. A transmissive boundary condition was used at the right-hand boundary to allow water to pass out of the solution domain.

Data were collected from two points within the solution domain. At $x = 1.0$ m, the water surface elevation was recorded which corresponds with the gauge placed 1.0 m from the battered wall. At $x = 2.03$ m, the overtopping discharge, q, was calculated from the water depth and positive velocity by using the equation

$$q = hu\Delta t. \tag{12}$$

An overtopping event is considered to have occurred if a positive water depth is recored at the gauge

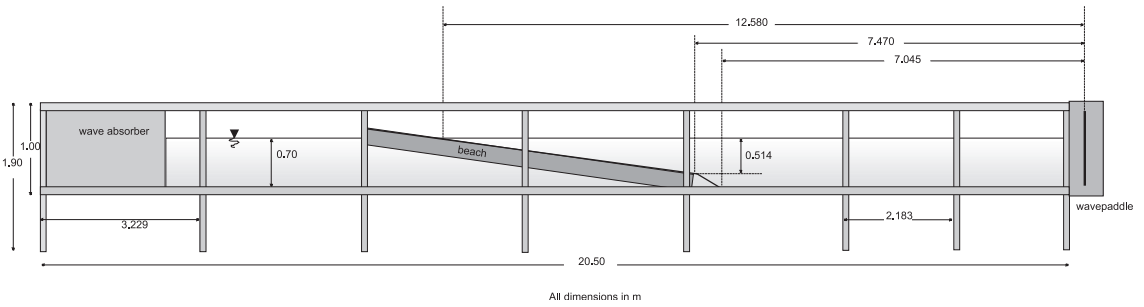

Fig. 2. Edinburgh wave flume: side elevation.

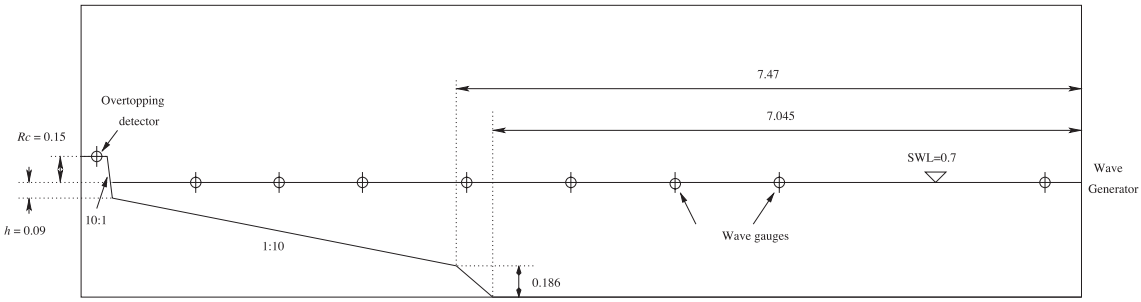

Fig. 3. Edinburgh wave flume: experimental setup.

placed at the top of the battered wall and the velocity recorded at the same gauge is landward.

3.3. Results

A plot of the numerical and experimental water surface at the gauge placed 1.0 m away from the battered wall over two separate time intervals can be seen in Fig. 4. A comparison between the water surface elevation for the physical model and the numerical model suggests that the numerical surface over-predicts the wave heights at the gauge placed 1.0 m away from the battered wall. The crests of the numerical waves occur at the same time as the physical waves. The lack of dispersion within the SWE is responsible for this shortfall in the numerical model as the energy loss observed in the physical model is not replicated.

Plots showing the overtopping discharge, q, over time 0–1200 s for all 15 runs of the numerical model and the physical model can be seen in Figs. 5 and 6. An overtopping event can be identified in Figs. 5 and 6 to be a steep upward turn in the discharge plot. Runs 3, 13 and 14, in particular, show excellent agreement between the numerical and physical discharge. However, runs 7, 9 and 10 show that the agreement is poor for these cases. A quantitative analysis of the discharges has been performed in Section 3.4.

Table 1
Edinburgh wave flume experiment parameters

Run	$H_s^{\dagger}$	$T_m^{\dagger}$	h*	R_h
1	0.063	1.23	0.0544	0.1296
2	0.074	1.27	0.0435	0.0881
3	0.069	1.25	0.0481	0.1046
4	0.059	1.25	0.0563	0.1431
5	0.062	1.25	0.0536	0.1296
6	0.071	1.50	0.0325	0.0686
7	0.078	1.48	0.0304	0.0584
8	0.063	1.52	0.0356	0.0849
9	0.050	1.52	0.0449	0.1347
10	0.075	1.50	0.0307	0.0615
11	0.062	0.97	0.0889	0.2152
12	0.059	0.95	0.0974	0.2477
13	0.066	0.98	0.0818	0.1860
14	0.068	1.00	0.0763	0.1683
15	0.064	0.98	0.0844	0.1978

† Measured at the toe of the battered wall.

3.4. Wave and overtopping statistics

In order to compare the numerical model of the wave flume and the physical experiment, a number of statistics have been calculated that analyse the water surface elevations and the overtopping discharges. To compare the water surface elevations recorded by the depth gauges placed 1.0 m away from the battered wall, the probability density functions (PDFs) for numerical and physical models have been calculated and compared with the Rayleigh distributions. Analysis of the overtopping discharges has been achieved by calculating values of dimensionless parameters and comparing results against empirical formulae.

3.4.1. Rayleigh wave height distribution

Longuet-Higgins (1952) showed that based upon the linear model of waves with a narrow energy spectrum, wave heights in deep water should follow the Rayleigh distribution (Battjes and Groenendijk,

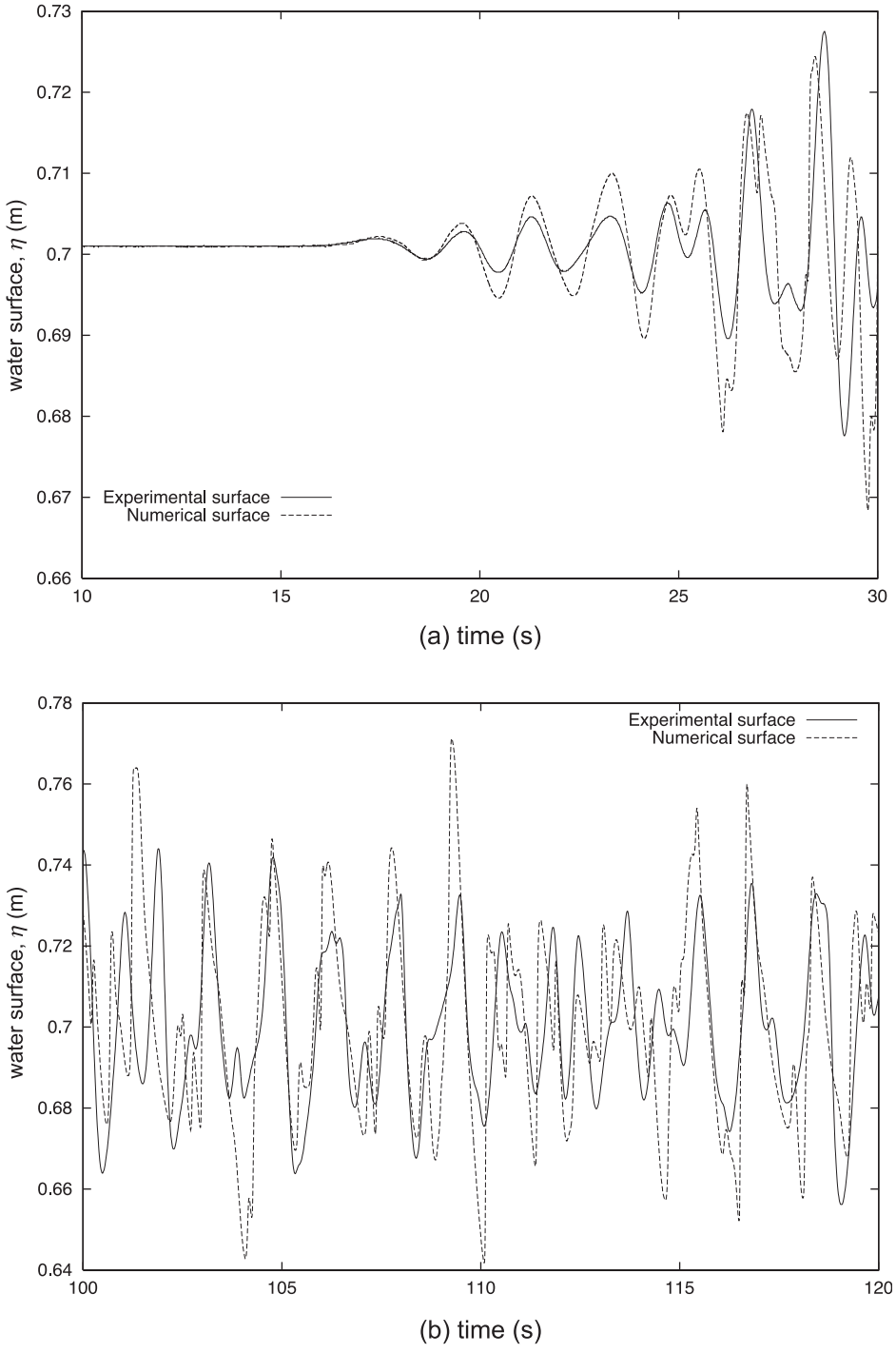

Fig. 4. Numerical simulation of the Edinburgh wave flume experiments: comparison of the experimental (solid line) and the numerical (dotted line) water surface at gauge placed 1.0 m from the battered wall over time intervals of t=[10,30] (a) and t=[100,120] (b).

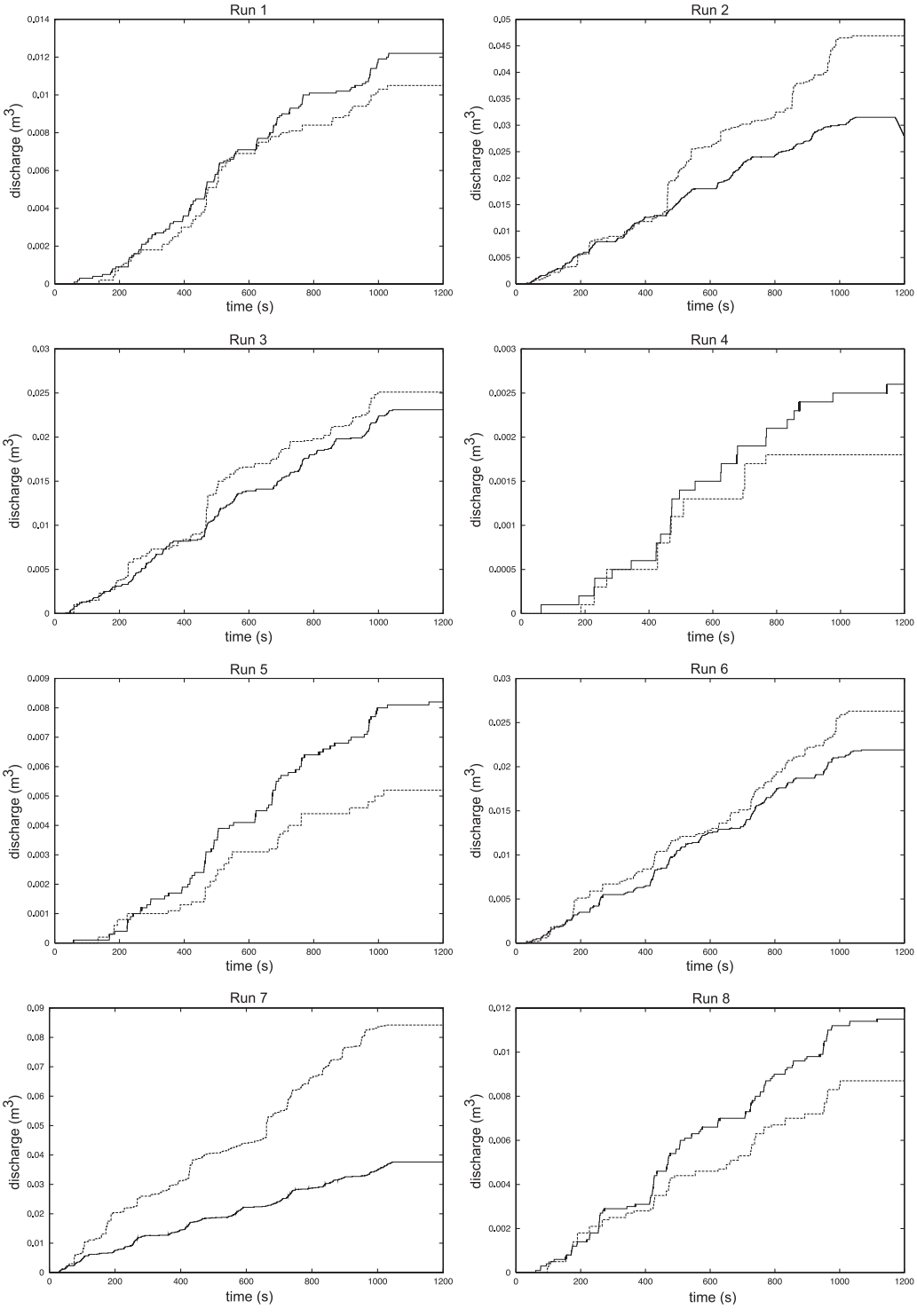

Fig. 5. Comparison of the numerical discharge (dotted line) against the experimental discharge (solid line) for runs 1–8.

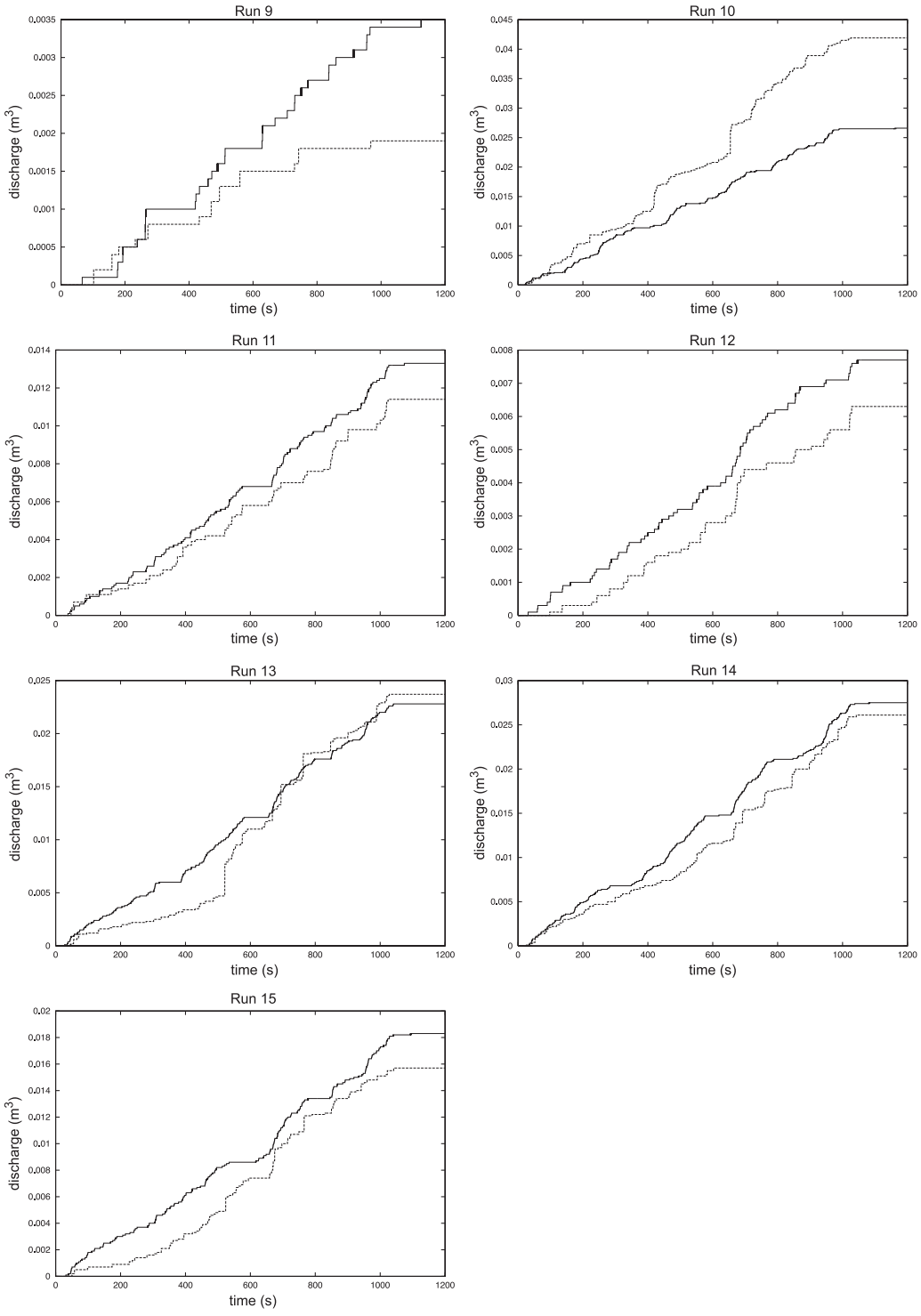

Fig. 6. Comparison of the numerical discharge (dotted line) against the experimental discharge (solid line) for runs 9–15.

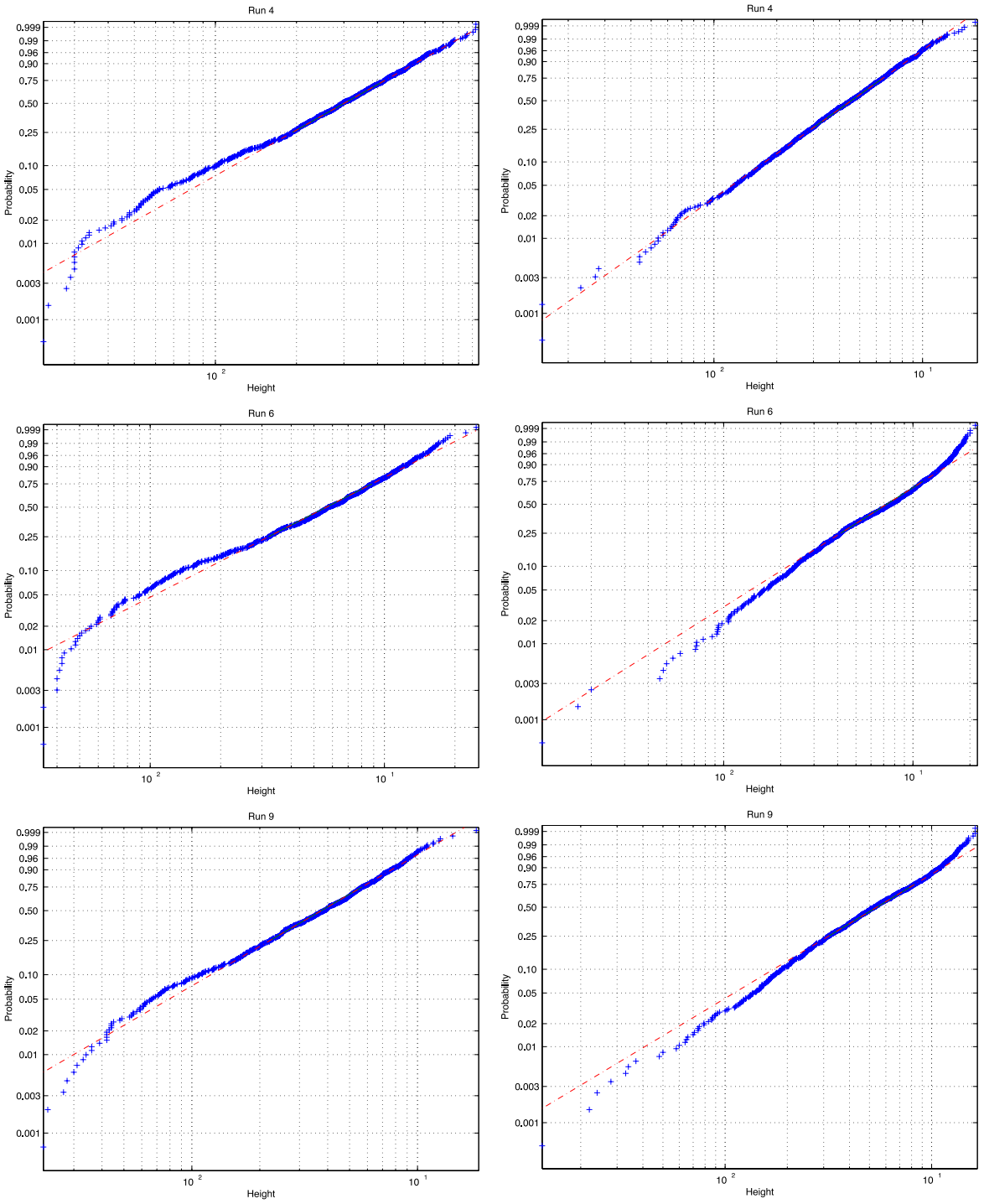

Fig. 7. Comparison of the experimental (left) and numerical (right) PDFs against their corresponding Rayleigh distributions (dashed line) for runs 4, 6 and 9.

2000). The probability that waves have a height less than H is then

$$P(\underline{H} < H) = 1 - \exp\left[-\left(\frac{H}{H_{\text{rms}}}\right)^2\right], \quad (13)$$

where $\underline{H}$ is a random variable; $H_{\text{rms}} = H_{1/3}/1.416$ is the root mean square (rms) of the wave heights, and $H_{1/3}$ is the mean of the top 1/3 wave heights.

The observed probability distribution for the wave heights is given as

$$P(\underline{H} < H) = 1 - \frac{i}{N-1}, \quad (14)$$

where i is the ith largest recorded wave height and N is the number of waves recorded. Plots of the observed and Rayleigh probability functions for runs 4, 6 and 9 are compared in Fig. 7.

The observed probability functions for both the physical experiment and the numerical model closely follow the Rayleigh distribution when the observed wave heights are greater than the median value. For smaller wave heights, there is a degree of scatter away from the Rayleigh probability distribution. However, as noted earlier (Fig. 4), the numerical model produces greater wave heights.

3.4.2. Overtopping statistics

In order to compare overtopping discharges between different experimental set-ups, dimensionless parameters for the volume of discharge and freeboard have been calculated. For h^* values of less than 0.3, these are given as (Besley, 1999)

$$Q_h = \left(\frac{Q}{\sqrt{gH_s^3}}\right)/h^{*2}, \quad (15)$$

and

$$R_h = \left(\frac{R_c}{H_s}\right)h^*, \quad (16)$$

where H_s is the significant wave height at the toe of the battered wall, Q_h is the dimensionless discharge and R_h is the dimensionless freeboard; Q is the mean overtopping discharge rate per metre of sea wall (q/t where t denotes the total amount of time the experiments was run for, in this case $t = 1200$ s), and R_c is the crest freeboard (Fig. 2). Besley et al. (1998) performed an extensive range of measurements for mean overtopping discharge on vertical walls, and the line of best fit using these measurements can be described by the following equation

$$Q_h = 0.000137R_h^{-3.24}. \quad (17)$$

Besley also developed an equation describing the proportion of waves that overtop a vertical wall given

Table 2
Overtopping statistics

Run	h^*	Physical model					Numerical model				
		Q	Q_h	N_{ow}	N_w	N_{ow}/N_w (%)	Q	Q_h	N_{ow}	N_w	N_{ow}/N_w (%)
1	0.063	1.26E − 05	0.0502	175	863	20	1.09E − 05	0.0436	84	1037	8
2	0.074	3.25E − 05	0.2033	479	888	54	5.02E − 05	0.3142	290	967	30
3	0.069	2.38E − 05	0.1216	299	900	33	2.70E − 05	0.1379	196	1017	19
4	0.059	2.68E − 06	0.0100	39	850	5	1.24E − 06	0.0046	13	1038	1
5	0.062	8.45E − 06	0.0349	132	898	15	6.19E − 06	0.0255	44	1042	4
6	0.071	2.26E − 05	0.2531	329	719	46	2.40E − 05	0.2693	203	854	24
7	0.078	3.88E − 05	0.4971	535	712	75	8.83E − 05	1.1317	541	847	64
8	0.063	1.19E − 05	0.1104	173	682	25	9.49E − 06	0.0883	61	861	7
9	0.050	3.61E − 06	0.0212	76	658	12	2.17E − 06	0.0127	14	849	2
10	0.075	2.74E − 05	0.3431	410	719	57	4.87E − 05	0.6088	292	864	34
11	0.062	1.37E − 05	0.0205	204	1000	20	1.11E − 05	0.0167	89	1252	7
12	0.059	7.94E − 06	0.0099	125	1017	12	6.91E − 06	0.0086	47	1239	4
13	0.066	2.35E − 05	0.0415	394	985	30	2.61E − 05	0.0460	150	1233	12
14	0.068	2.84E − 05	0.0576	357	1000	36	2.63E − 05	0.0534	214	1225	17
15	0.064	1.89E − 05	0.0313	278	985	28	1.63E − 05	0.0270	121	1239	10

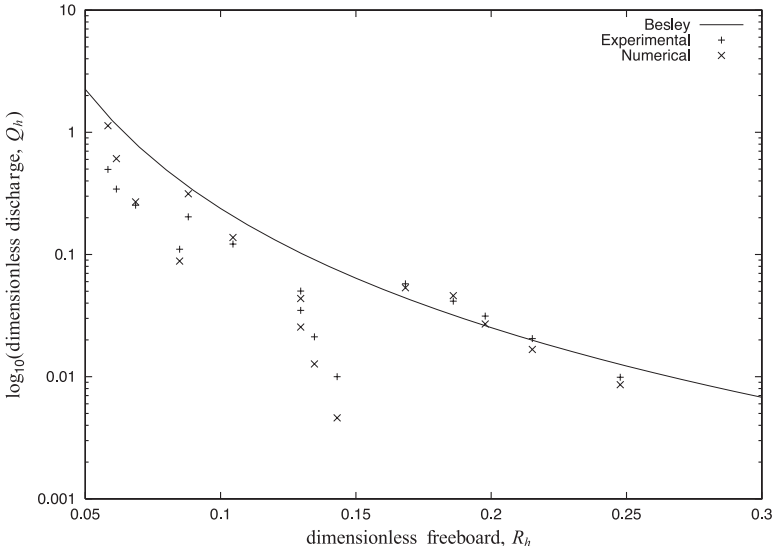

Fig. 8. Dimensionless discharge (Q_h) plotted against dimensionless freeboard (R_h) for the physical model and the numerical model.

the dimensionless freeboard parameter. For $h^* \leq 0.3$, this is

$$N_{ow}/N_w = 0.031 R_h^{-0.99}, \quad (18)$$

where N_{ow} is the number of overtopping waves, and N_w is the number of waves in the sequence.

Table 2 contains the overtopping statistics calculated for both the physical and numerical models. The dimensionless discharges are plotted against the dimensionless freeboards in Fig. 8 which also shows Besley's relationship. The percentages of waves overtopping in the numerical and physical models are shown in Fig. 9, along with the empirical Besley curve.

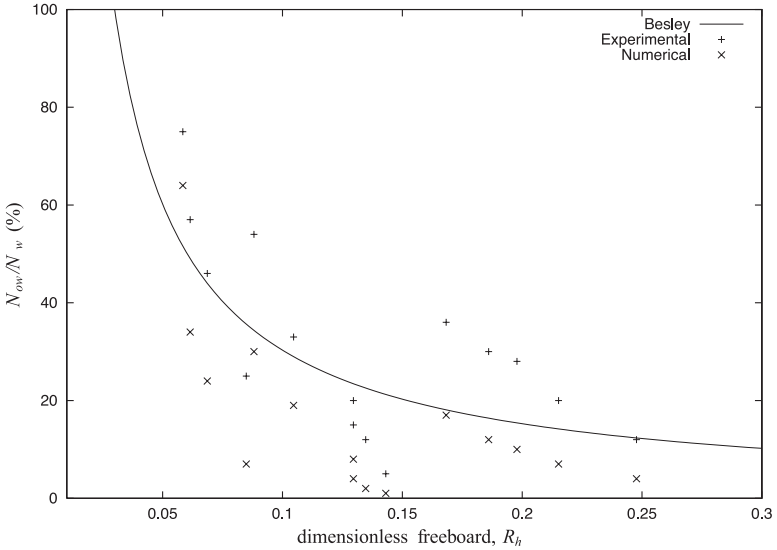

Fig. 9. Percentage of waves overtopping the 10:1 battered wall.

For dimensionless freeboard values of 0.16 and greater, there is excellent agreement both between the numerical and experimental dimensionless discharges and with the Besley curve (Fig. 8). At the lower values of R_h ($R_h \leq 0.1$), there is not so good agreement between the two data sets and the Besley curve. However, the general trend is still maintained. For R_h between 0.12 and 0.15, there is a marked decrease in the accuracy of the Besley curve when compared to the calculated dimensionless discharges.

The percentage of waves overtopping in the numerical model is significantly less than was recorded from the physical model (Fig. 9). This is due to the fact that breaking waves are represented by bore waves in the depth averaged SWE. The physical processes that occur to create violent overtopping events cannot be modelled properly in this manner, hence, the wave-by-wave overtopping predictions. However, as a comparison of the discharge volume shows, the SWE give good predictions of mean overtopping discharge. In keeping with the findings from Fig. 8, where the R_h values are greater than 0.16, the numerical model shows slightly better agreement with the Besley curve than at lower values of R_h where the data points are more scattered.

The absolute percentage difference between the numerical and the physical models has been calculated for both the dimensionless discharge and the significant wave height 1.0 m from the battered wall (Fig. 10). Fig. 10 shows that there are two distinct populations of data points, the runs where the h^* values are 0.075–0.1 and the runs where the h^* values are less than 0.06. For runs where the h^* parameter is 0.075–0.1 (runs 11–15), the percentage errors for both the dimensionless discharge (Q_h) and the significant wave heights (H_s) are less than 20%. For the runs where the h^* parameter is less than 0.06 (runs 1–10), the absolute percentage error for the significant wave height is typically 35–40%, and the percentage error for the dimensionless discharge is also spread around the 35–40% area, with two outliers that have a percentage error of 79% and 127% where the value of h^* is the lowest of all of the runs at 0.03.

4. Conclusions

AMAZON, a numerical model based upon the shallow water equations was described. The numerical scheme used is the MUSCL–Hancock scheme which is a high-resolution Godunov-type scheme that uses MUSCL reconstruction to prevent spurious oscillations. The surface gradient method, a modern method for dealing with the treatment of source terms within

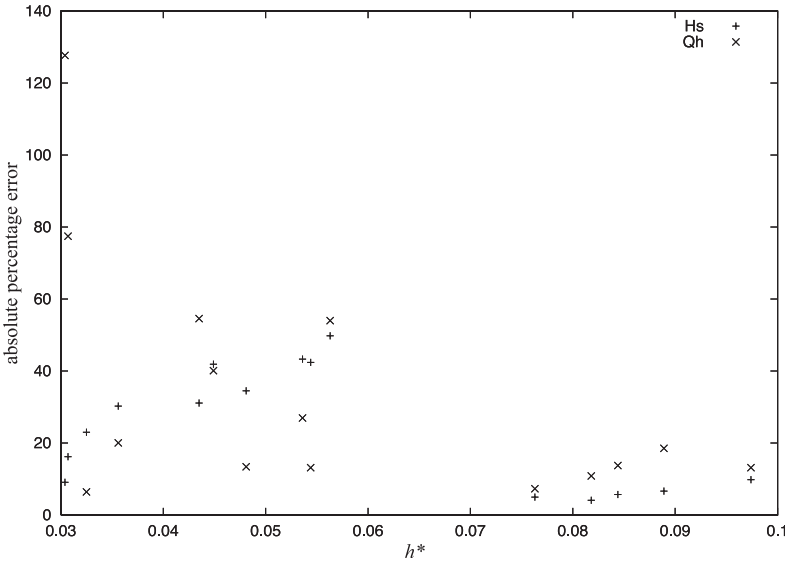

Fig. 10. Percentage error between the physical model and the numerical model for the observed significant wave height (H_s) and the dimensionless discharge (Q_h).

the shallow water equations, was discussed and implemented. The numerical model was used to simulate a physical experiment carried out in a wave flume as part of the VOWS project.

Comparisons between water surface elevations of the physical and numerical models show that although the waves occur at the same time, the numerical surface over-predicts the heights of each wave. This can be attributed to the lack of dispersion within the shallow water equations that are being used in non-shallow water. The probability density functions for non-exceedence were calculated for both the physical and numerical models and compared against the expected Rayleigh distributions. Both models showed good agreement with the expected Rayleigh distributions, but again showed that the numerical model over-predicts the wave heights.

Dimensionless statistics were calculated to compare overtopping discharges. These were then compared to empirical formulae that showed that for higher h^* values, there was better agreement between the numerical model, the physical model and the empirical formulae. An analysis of the percentage of overtopping waves showed that the numerical model significantly underestimated the number of overtopping events in the sequence, but it was noted that for higher values of R_h (and therefore, h^*) the numerical model provided a better fit to the empirical formulae than for lower values of h^*. Finally, a comparison was made between the absolute percentage error between the numerical and physical model that showed that for h^* values 0.075–0.1, the shallow water equations produce results to within 20% of the physical model for both the significant wave height and the dimensionless discharge. For values of h^* below 0.06, the analysis showed that the percentage errors ranged from a typical 40% to a couple of outliers at 79% and 127% for small values of h^* where waves are mostly impacting.

It is concluded that the shallow water equations provide a useful alternative to more computationally expensive models for violent wave overtopping provided the h^* parameter does not fall below 0.075 and that the seaward boundary condition is sufficiently close to the structure. This model provides a useful engineering design tool with 1000 wave simulations taking less than two minutes to run on a moderately fast PC. Further work to extend the model to include dispersive terms, helping to eliminate differences between the physical and numerical wave heights, will allow the seaward boundary to be located further offshore.

Acknowledgements

The authors would like to thank Dr. Jonathan Pearson and Prof. William Allsop for their invaluable contribution to the VOWS project and for providing the experimental data. The VOWS project was funded by the EPSRC under two linked grants, numbers GR/M 42312 and GR/M 42428. The authors also wish to acknowledge the helpful discussions on wave overtopping that have taken place within the EU-funded Framework-V project CLASH, contract number EVK3-CT-2001-00058.

References

Allsop, N.W.H., Besley, P., Madurini, L., 1995. Overtopping performance of vertical walls and composite breakwaters, sea walls and low reflection alternatives. Tech. rep., Paper 4.7 in MCS Final Report, University of Hanover.

Battjes, J.A., Groenendijk, H.W., 2000. Wave height distributions on shallow foreshores. Coastal Engineering 40, 161–182.

Besley, P., 1999. Overtopping of Sea walls—design and assessment manual. R&D Technical Report W178. Tech. rep., Environment Agency, Bristol.

Besley, P., Stewart, T., Allsop, N.W.H., 1998. Overtopping of vertical structures: new methods to account for shallow water conditions. Proceedings of International Conference on Coastlines, Structures and Breakwaters '98, Institution of Civil Engineers, London, pp. 46–57.

Davis, S.F., 1988. Simplified second-order Godunov-type methods. SIAM Journal of Statistical and Scientific Computing 9, 445–473.

Dodd, N., 1998. A numerical model of wave runup, overtopping and regeneration. Proc. ASCE Journal of Waterways, Port and Coastal Engineering 124 (2), 73–81.

Fraccarollo, L., Toro, E.F., 1995. Experimental and numerical assessment of the shallow water model for two dimensional dam-break type problems. Journal of Hydraulic Research 33, 843–864.

Franco, L., de Gerloni, M., van der Meer, J., 1994. Wave overtopping on vertical and composite breakwaters. Proceedings from 24th International Conference on Coastal Engineering, Kobe, ASCE, New York.

Garcia-Navarro, P., Vázquez-Cendón, M.E., 2000. On numerical treatment of the source terms in the shallow water equations. Computers and Fluids 29, 951–979.

Goda, Y., Kishira, Y., Kamiyama, Y., 1975. Laboratory investigation on the overtopping rates of sea walls by irregular waves. Ports and Harbour Research Insitute, Yokosuka 14, 3–44.

Harten, A., Lax, P., van Leer, B., 1983. On upstream differencing and Godunov-type schemes for hyperbolic conservation laws. SIAM Review 25, 35–61.

Hirsch, C., 1998. Numerical Computation of External and Internal Flows, vol. 1. Wiley, Chichester, UK.

Hu, K., Mingham, C.G., Causon, D.M., 2000. Numerical simulation of wave overtopping of coastal structures using the non-linear shallow water equations. Journal of Coastal Engineering 41, 433–465.

Leveque, R.J., 1998. Balancing source terms and flux gradients in high-resolution Godunov methods: the quasi steady wave propagation algorithm. Journal of Computational Physics 146, 346–365.

Longuet-Higgins, M.S., 1952. On the statistical distributions of heights of sea waves. Journal of Marine Research 11, 245–266.

Mingham, C.G., Causon, D.M., 1998. High-resolution finite-volume method for shallow water flows. Journal of Hydraulic Engineering 124, 605–614.

Morton, K.W., Mayers, D.F., 1994. Numerical Solution of Partial Differential Equations. Cambridge Univ. Press, Cambridge, UK.

Owen, M., 1982. Overtopping of sea defences. Proceedings from Conference Hydraulic Modelling of Civil Engineering Structures, BHRA, University of Warwick, Coventry, pp. 469–480.

Pearson, J., Bruce, T., Allsop, N.W.H., 2001. Prediction of wave overtopping at steep sea walls—variabilities and uncertainties. Proceedings Waves'01. ASCE, San Francisco, pp. 1797–1808.

Peregrine, D.H., 2002. Water wave impact on walls. Annual Reviews of Fluid Mechanics 35, 23–43 (in press).

Richardson, S.R., Ingram, D.M., Mingham, C.G., Causon, D.M., 2001. On the validity of the shallow water equations for violent overtopping. Ocean Wave Measurement and Analysis, Proceedings Waves'01, vol. 2. ASCE, Reston VA, pp. 1112–1125.

Toro, E.F., 1997. Riemann Solvers and Numerical Methods for Fluid Dynamics. Springer-Verlag, Berlin.

van Gent, M., 1994. Modelling of wave action on and in coastal structures. Coastal Engineering 22.

van Gent, M., 1995. Wave interaction with permeable coastal structures. PhD thesis, Delft University, pp. 311–339.

van Leer, B., 1985. On the relation between the upwind-differencing schemes of Godunov, Enguist–Osher and Roe. SIAM Journal of Scientific and Statistical Computing 5, 1.

Zhou, J.G., Causon, D.M., Mingham, C.G., Ingram, D.M., 2001. The surface gradient method for the treatment of source terms in the shallow water equations. Journal of Computational Physics 168, 1–25.